AGU100 ADVANCING EARTH AND SPACE SCIENCE

Journal of Advances in Modeling Earth Systems

RESEARCH ARTICLE

10.1002/2017MS001196

Methane Feedback on Atmospheric Chemistry: Methods, Models, and Mechanisms

Christopher D. Holmes[1]

[1]Earth, Ocean and Atmospheric Science, Florida State University, Tallahassee, Florida, USA

Key Points:

- Theory and applications of the atmospheric CH_4 feedback are reviewed, with emphasis on practical methods and their limitations
- The CH_4 feedback varies spatially and seasonally, which can be understood from HO_x family partitioning and production
- The CH_4 feedback, perturbation time, and environmental impacts have likely grown over the industrial era and continue to rise

Supporting Information:

- Figure S1
- Data Set S1

Correspondence to:
C. D. Holmes,
cdholmes@fsu.edu

Citation:
Holmes, C. D. (2018). Methane feedback on atmospheric chemistry: Methods, models, and mechanisms. *Journal of Advances in Modeling Earth Systems*, *10*. https://doi.org/10.1002/2017MS001196

Received 9 OCT 2017
Accepted 27 MAR 2018
Accepted article online 6 APR 2018

Abstract The atmospheric methane (CH_4) chemical feedback is a key process for understanding the behavior of atmospheric CH_4 and its environmental impact. This work reviews how the feedback is defined and used, then examines the meteorological, chemical, and emission factors that control the feedback strength. Geographical and temporal variations in the feedback are described and explained by HO_x ($HO_x = OH + HO_2$) production and partitioning. Different CH_4 boundary conditions used by models, however, make no meaningful difference to the feedback calculation. The strength of the CH_4 feedback depends on atmospheric composition, particularly the atmospheric CH_4 burden, and is therefore not constant. Sensitivity tests show that the feedback depends very weakly on temperature, insolation, water vapor, and emissions of NO. While the feedback strength has likely remained within 10% of its present value over the industrial era and likely will over the twenty-first century, neglecting these changes biases our understanding of CH_4 impacts. Most environmental consequences per kg of CH_4 emissions, including its global warming potential (GWP), scale with the perturbation time, which may have grown as much as 40% over the industrial era and continues to rise.

Plain Language Summary Methane emissions alter atmospheric chemistry in ways that amplify the impact of those emissions. This work examines the chemical and meteorological causes of that feedback. The feedback and environmental impacts of CH_4 emissions have likely strengthened over the historical era.

1. Introduction and Review

Methane (CH_4) is a major greenhouse gas; its emissions are responsible for about 1 W m^{-2} of radiative forcing in 2011 (Myhre et al., 2013). Chemical oxidation of CH_4 in the atmosphere is therefore a critical climate process, removing one major greenhouse gas and producing several others: CO_2, H_2O, and O_3. Quantifying this process and how it responds to perturbations is a central task of atmospheric chemistry models. One important effect of CH_4 on atmospheric chemistry is controlling concentrations of tropospheric hydroxyl radicals (OH), a key oxidant in the atmosphere. CH_4 is removed from the atmosphere mainly by reacting with OH:

$$CH_4 + OH \xrightarrow{O_2} CH_3O_2 + H_2O. \tag{1}$$

CH_4 is also removed by soil uptake and reactions with atomic chlorine and stratospheric oxidants, but these losses are small. Although subsequent reactions with CH_3O_2 regenerate OH (Lelieveld et al., 2016; Wennberg et al., 1998), the net effect is that CH_4 suppresses tropospheric OH concentrations, prolongs the CH_4 lifetime, and amplifies the CH_4 concentration response to emission changes. This is known as the CH_4 feedback effect and it increases the radiative forcing, global warming potential, and environmental impact of CH_4 emissions.

This paper combines a literature review of the CH_4 feedback with new research results. The remainder of section 1 reviews and summarizes the core theory, analysis methods, and applications of the CH_4 feedback. These equations and results are gathered from many papers and presented together for the first time (Berntsen et al., 1992; Fuglestvedt et al., 1996, 1999; Prather, 1994, 1996, 2002, 2007; West et al., 2007; Wild & Prather, 2000). In some cases, I provide derivations and discussion of implicit assumptions that were not present in the original literature. Sections 2 and 3 use a global atmospheric chemistry model to probe previously unexamined aspects of the CH_4 feedback: its spatial and temporal variation; the influence of meteorology, emissions, and atmospheric composition; and the role of model boundary conditions.

1.1. Behavior of a Mass Perturbation

The essential dynamics of the CH_4 feedback can be derived from the mass balance equation

$$\frac{dm}{dt} = E - km \tag{2}$$

where m is the mass or burden of CH_4 in the atmosphere, E is the emission rate, and k is the first-order loss frequency due to all processes. Averaging each term over 1 year or more avoids complications of seasonal cycles. We can linearize equation (2) around the steady state with emissions E_0, loss frequency k_0, and mass $m_0 = E_0/k_0$ to determine the behavior of a small perturbation $m' = m - m_0$. Since OH concentrations depend on the CH_4 abundance (reaction (1)), the loss frequency k with the perturbed mass is $k = k_0 + m'(dk/dm)$. The CH_4 perturbation is governed by

$$\frac{dm'}{dt} = -k_0(1+R)m'; \quad R \equiv \frac{dk/k_0}{dm/m_0} = \frac{d\ \ln k}{d\ \ln m} \tag{3}$$

plus neglected terms of order m'^2. R represents the fractional change in CH_4 loss frequency per fractional change in atmospheric CH_4 abundance, which must be negative since rising CH_4 abundance suppresses OH and CH_4 loss. The solution to this equation is $m'(t) = m'(0)\exp\left(-t/\tau_p\right)$, where τ_p is the perturbation time scale

$$\tau_p = \frac{1}{k_0(1+R)} = f\tau_0; \quad f \equiv \left(\frac{1}{1+R}\right). \tag{4}$$

f is generally called the feedback factor. In reality, CH_4 mass perturbations follow a more complex decay curve with multiple e-folding time scales, due to coupling with CO, O_3, and other reactive gases that is not fully accounted for in reaction (1) (Prather, 1994). Nevertheless, they result in a time-average perturbation identical to that derived here (Prather, 2002) and the single perturbation time τ_p above is very close to the slowest mode that dominates in the fully coupled system (Prather, 1994).

Past studies have found $R \approx -0.25$ to -0.3 and $f \approx 1.3$–1.4 (Fiore et al., 2009; Holmes et al., 2013; Prather et al., 2001; Stevenson et al., 2013), meaning that CH_4 perturbations persist 1.3–1.4 times longer than would be expected from the steady state lifetime τ_0 derived from the CH_4 budget. For chemical box models or low-dimensional spatial models, the perturbation time τ_p can be derived analytically from eigen-analysis of the chemical Jacobian, but this approach is intractable for state-of-the-art global models with order 10^8 chemical state variables. For these models, the feedback must be derived from numerical evaluation of R or other methods described below.

The distinction between lifetime and perturbation time is important for the cumulative radiative forcing (RF), or climate heating, from a CH_4 emission pulse, among other impacts (Fuglestvedt et al., 1996, 1999; Prather, 2002):

$$\int_0^T RF(t)\ dt = E_{RF}\ m'(0)\int_0^T \exp\left(-t/\tau_p\right)dt = E_{RF}m'(0)\tau_p\left(1-e^{-T/\tau_p}\right), \tag{5}$$

where E_{RF} is the specific radiative forcing from 1 kg of CH_4. If $m'(0) = 1$ kg, then this quantity is the absolute global warming potential ($AGWP_{CH_4}$). The global warming potential (GWP) of CH_4 is then the ratio of $AGWP_{CH_4}$ to the AGWP of CO_2. If $T \gg \tau_p$, as is the case for the 100-year AGWP and longer, then

$$AGWP_{CH_4} = E_{RF}f\tau_0. \tag{6}$$

This demonstrates that it is the perturbation time, $\tau_p = f\tau_0$, not the lifetime, τ_0, that determines the GWP, climate, and environmental effects of CH_4.

1.2. Behavior of Emission or Loss Perturbations

The feedback effect also influences the change in steady state mass in response to a sustained change in emissions. An emissions change, dE, initially creates a proportional change in steady state mass

$$\frac{dm_1}{m_0}=\frac{dE}{E_0}. \tag{7}$$

While this would be exact for a linear system with constant k_0, the mass change dm_1 alters the loss frequency

$$\frac{dk_1}{k_0}=R\frac{dm_1}{m_0}. \tag{8}$$

The new loss frequency, in turn, creates a secondary change in steady state mass

$$\frac{dm_2}{m_0}=-\frac{dk_1}{k_0}=-R\frac{dm_1}{m_0}=-R\frac{dE}{E_0}. \tag{9}$$

Tertiary and higher changes follow $dm_n/m_0=(-R)^{n-1}(dE/E_0)$ so the full perturbation to the burden in response to a change in emissions is a geometric series

$$\frac{dm}{m_0}=\frac{dm_1}{m_0}+\frac{dm_2}{m_0}+\frac{dm_3}{m_0}+\ldots=\frac{dE}{E_0}\left(1-R+R^2-\ldots\right)=f\frac{dE}{E_0}. \tag{10}$$

The same result can also be obtained from the steady state condition, $E=km$. Dividing its total differential, $dE=k\ dm+m\ dk$, by the original steady state, $E_0=k_0m_0$, and substituting R from equation (3) leads to equation (10). Thus, the same feedback factor, f, describes both the prolonged decay of a mass perturbation (equations (3) and (4)) as well as the amplified mass response to a sustained emission change (equation (10)). Exogenous changes in CH_4 lifetime or loss rate—via changes in O_3 precursors, weather, or climate—can also trigger a change in steady state mass. In that case equations (7)–(10) still apply with dE/E_0 replaced by $d\tau/\tau_0$or$-dk/k_0$.

1.3. Large CH_4 Perturbations

The discussion and all equations above began from the premise that the CH_4 perturbations are small. Specifically, equations (3) and (8) estimate changes in loss frequency using only the first derivative. Therefore, nearly all of the subsequent results, including the perturbation lifetime (equation (4)), feedback factor, and new steady state mass (equation (10)), strictly apply only for small or infinitesimal CH_4 perturbations. For large emission changes, results may differ from these linearized equations above because R varies with the CH_4 burden and other emissions. Section 3.2 critically examines the stability of R and f, but for some purposes R can be treated as constant.

To determine the steady sate mass change expected from a finite change in emissions from E_a to E_b, equation (10) can be integrated

$$\int_{m_a}^{m_b}\frac{dm}{m}=\int_{E_a}^{E_b}f\frac{dE}{E}. \tag{11}$$

If masses m_a and m_b differ by less than about 50%, then R and f can be treated as a constant (±5%; see section 3.2). In that case

$$\frac{m_b}{m_a}=\left(\frac{E_b}{E_a}\right)^f. \tag{12}$$

Following the same reasoning, if the change is initiated by an exogenous change in loss rate or lifetime from $\tau_a=1/k_a$ to $\tau_b=1/k_b$, then the masses are related by (West et al., 2007)

$$\frac{m_b}{m_a}=\left(\frac{\tau_b}{\tau_a}\right)^f=\left(\frac{k_a}{k_b}\right)^f. \tag{13}$$

Note that the ratios $\tau_b/\tau_a=k_a/k_b$ represent only the initial exogenous change in CH_4 loss while holding CH_4 concentrations constant. The losses and lifetimes will be further modified by the feedback effect. Both equations (12) and (13) should be restricted to situations where f is approximately constant. For greater realism, section 3.2 defines f as a function of CH_4 burden, which enables numerical integration of equation (11) without approximating f as constant.

1.4. Methods for Quantifying CH_4 Feedback From Chemical Models

Although observations of CH_3CCl_3 and some other gases constrain the CH_4 lifetime τ (Montzka et al., 2011; Rigby et al., 2017; Spivakovsky et al., 2000; Turner et al., 2017), there are no observations that directly constrain τ_p or $f=\tau_p/\tau$. Global atmospheric chemistry models provide the only feasible means of quantifying these important quantities. The simplest approach to estimate τ_p is to perturb the mass of CH_4 in a model and fit the simulated mass decay to an exponential function (Derwent et al., 2001; Wild & Prather, 2000). While this method works, it is rarely used because it requires two simulations (control and perturbation) lasting a decade or more to obtain a good estimate of τ_p and $f=\tau_p/\tau$. The derivation above suggests a more efficient method is to calculate R from two short simulations with different CH_4 burdens; then f and τ_p are calculated via equation (4). This is the approach established by Prather et al. (1995) and used by most researchers since (Fuglestvedt et al., 1999; Prather et al., 2001; Fiore et al., 2009; Holmes et al., 2013; Stevenson et al., 2013; Voulgarakis et al., 2013).

In the standard approach, the CH_4 loss due to tropospheric OH (L_{OH}) and total atmospheric CH_4 mass (m) are diagnosed from a model representing the present-day atmosphere. The loss and mass should be averaged over at least 1 year to represent mean annual conditions, after several months of spin-up to approach steady state for tropospheric species, including O_3, CO, and C_2H_6. The partial loss frequency (k_{OH}) and lifetime (τ_{OH}) are derived from annual, global mean quantities

$$k_{\mathrm{OH}}=\frac{1}{\tau_{\mathrm{OH}}}=\frac{L_{\mathrm{OH}}}{m}. \tag{14}$$

The total CH_4 loss frequency (k) and lifetime (τ) must also account for CH_4 losses from tropospheric Cl (L_{Cl}), stratospheric oxidants (L_{strat}), and soil (L_{soil}):

$$k=\frac{1}{\tau}=\frac{L}{m}=\frac{L_{\mathrm{OH}}+L_{\mathrm{Cl}}+L_{\mathrm{strat}}+L_{\mathrm{soil}}}{m}=k_{\mathrm{OH}}+k_{\mathrm{Cl}}+k_{\mathrm{strat}}+k_{\mathrm{soil}}. \tag{15}$$

Literature values can be used for any process that is not simulated in the model. Reasonable values are $k_{\mathrm{Cl}}=0.005\ \mathrm{yr}^{-1}$, $k_{\mathrm{strat}}=0.0083\ \mathrm{yr}^{-1}$, and $k_{\mathrm{soil}}=0.0067\ \mathrm{yr}^{-1}$ (Prather et al., 2012). These values should always be reported because they impact the overall feedback strength diagnosed from the model. The simulation is run a second time using perturbed CH_4 concentrations, often 5–20% larger. The sensitivity R is calculated by finite difference

$$R=\frac{\ln k_1-\ln k_0}{\ln m_1-\ln m_0}=\frac{\ln\left(k_1/k_0\right)}{\ln\left(m_1/m_0\right)}, \tag{16}$$

where subscripts 0 and 1 indicate quantities from the control and perturbed simulations, respectively. The denominator of equation (16) equals the size of the imposed perturbation to CH_4 burden. Some studies report the partial sensitivity of tropospheric OH loss to CH_4 concentration (e.g., Prather et al., 1995, 2001)

$$R_{\mathrm{OH}}=\frac{d\ \ln k_{\mathrm{OH}}}{d\ \ln m}=\frac{\ln k_{\mathrm{OH},1}-\ln k_{\mathrm{OH},0}}{\ln m_1-\ln m_0}. \tag{17}$$

This quantity is not needed to calculate the CH_4 feedback effect but can be a useful model diagnostic and means to isolate the feedback on tropospheric OH from the feedbacks on stratospheric or other losses. R and R_{OH} are related by

$$R=\frac{R_{\mathrm{OH}}k_{\mathrm{OH}}+R_{\mathrm{Cl}}k_{\mathrm{Cl}}+R_{\mathrm{strat}}k_{\mathrm{strat}}+R_{\mathrm{soil}}k_{\mathrm{soil}}}{k_{\mathrm{OH}}+k_{\mathrm{Cl}}+k_{\mathrm{strat}}+k_{\mathrm{soil}}}. \tag{18}$$

There has been little effort to study CH_4 feedbacks on other CH_4 loss processes ($R_{Cl}, R_{strat}, R_{soil}$). The common approach of prescribing fixed values of k_{Cl}, k_{strat}, and k_{soil} in equations (15) and (16), while k_{OH} changes, implicitly assumes that these feedbacks are zero, but they may not be. While these other feedbacks are unknown, because of their small loss frequencies compared to OH, they would have to be very strong to meaningfully change the overall feedback R or f. The sensitivity can also be expressed in terms of lifetime instead of loss frequency

$$S = \frac{d\ \ln \tau}{d\ \ln m} = -\frac{d\ \ln k}{d\ \ln m} = -R. \tag{19}$$

2. Model Description

I use the GEOS-Chem global chemical transport model (v11-01, www.geos-chem.org) to examine how the CH_4 feedback responds to meteorology, emissions, and model boundary conditions. Simulations are conducted with the tropospheric chemistry mechanism (Parrella et al., 2012) and MERRA-2 meteorology at 4° × 5° horizontal resolution and 47 vertical layers (Gelaro et al., 2017). When simulating tropospheric oxidant chemistry, GEOS-Chem typically uses specified CH_4 concentrations in four latitude bands. Here the model is reconfigured to interactively simulate CH_4 concentrations using CH_4 emissions from Wecht et al. (2014). CH_4 losses are calculated from the simulated tropospheric OH concentrations (reaction (1)) and fixed loss frequencies (given in section 1.4) for Cl, stratospheric oxidants, and soils. Chemical reaction diagnostics are added to track the production and loss of OH, O_3, and each chemical intermediate in the oxidation of CH_4 to CO_2. A minor bug in lightning NO emissions is also fixed (L. Murray, personal communication, 2017). The chemical initial condition is taken from a prior multiyear simulation and the CH_4 distribution is rescaled to match the observed marine background of 1,775 ppb in January 2005 (Dlugokencky et al., 2017). The first year is treated as spin-up.

To assess how CH_4 boundary conditions influence the feedback effect, I configure the model with three different types of CH_4 boundary conditions: specified emissions (described above), specified mole fractions at the surface, and specified mole fractions everywhere. The emission-driven simulation runs first and its monthly mean CH_4 mole fractions are imposed in the other configurations, so that the CH_4 distributions are nearly identical in the control simulations of all three configurations. The influences of emissions and meteorology are assessed with additional simulations that have doubled CO emissions, doubled NO_x emissions ($NO_x = NO + NO_2$), 1 K increase in temperature, 20% increase in water vapor, or 20% increase in photolysis rates. These additional simulations all start in January 2006 and results for 2007 are analyzed. To calculate the feedback effect, one additional simulation is carried out in each configuration with the CH_4 emissions or mole fractions increased 20% compared to its control simulation. These perturbation simulations also begin with 20% higher CH_4 mole fractions so that they approach their new steady state faster.

3. Results

3.1. Influence of CH_4 Boundary Conditions

At the time the methods in section 1.4 were developed, most global tropospheric chemistry models prescribed CH_4 concentrations everywhere based on observations so that the model would have a reasonable CH_4 distribution despite inconsistencies between CH_4 sources and modeled sinks. This approach meant that m_0 and m_1 were specified by the user. Furthermore, the fractional perturbation to CH_4 mole fractions was applied uniformly in all grid cells. Today, many models simulate CH_4 from its sources and sinks or using surface CH_4 mole fractions. In these models, the user controls only the surface abundance or fluxes, so m_0 and $d\ln m$ are outside the user's direct control. In addition, the fractional change in CH_4 mole fraction can vary throughout the model domain. This diversity of modeling approaches is found in several recent ensemble studies (Fiore et al., 2009; Stevenson et al., 2013; Voulgarakis et al., 2013). To date, it has not been demonstrated if or how these differences in model structure affect the CH_4 lifetime or its chemical feedback.

Table 1
CH_4 Loss Rates and Feedback Simulated With Different CH_4 Boundary Conditions[a]

	All fixed	Fixed surface	Surface emission
OH lifetime (year)	8.321	8.321	8.323
Total lifetime (year)	7.133	7.134	7.135
CH_4 mass 2007 (Tg)	4,474	4,476	4,479
CH_4 mass change[b] (Tg)	895	897	945
R_{OH}	−0.3159	−0.3160	−0.3179
R	−0.2697	−0.2698	−0.2714
F	1.369	1.370	1.372

[a] Numerical values are provided with four digits of precision to show the small differences between model configurations. CH_4 masses are lower than observational constraints because of the short CH_4 lifetime in the model. [b] Difference in 2007 between the control simulation and perturbation with 20% increase in the CH_4 boundary condition.

Table 1 compares the CH_4 lifetime and feedback under three different types of CH_4 boundary conditions. All three configurations produce nearly the same atmospheric chemical state by design. The differences in CH_4 burden are 0.07% and differences in CH_4 lifetime are 0.02%. In all cases, the CH_4 lifetime is shorter than suggested by observations (9.5 ± 1.3 year, Prather et al., 2012) because the model lacks some halogens (Sherwen et al., 2016), has coarse resolution

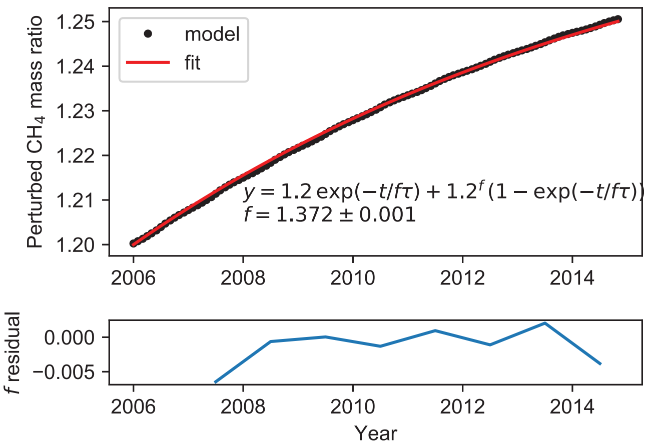

Figure 1. (top) Ratio of CH_4 mass in the perturbation and control simulations and (bottom) residual variability in feedback f after removing the effect of rising CH_4 mass via equation (20). In the top plot, feedback factor f is determined by fitting the ratio with an exponential approach to steady state.

(Holmes et al., 2013), and may misrepresent other processes, such as errors in the chemical mechanism or the influence of clouds and aerosols. Many other global atmospheric models also have similar magnitude and longstanding errors in CH_4 lifetime for reasons that remain unclear (e.g., Prather et al., 2001; Voulgarakis et al., 2013).

While the control simulations for each configuration are nearly identical, the perturbation simulations for each case are subtly different. In the configuration with fixed mole fractions everywhere, the vertical and spatial gradients of CH_4 cannot change from the control simulation and the CH_4 mole fractions rise exactly 20% everywhere. In the configurations with emissions or specified surface mole fraction, however, the CH_4 gradients and total mass are free to vary; inhomogeneity up to 1.5% of the perturbation magnitude arises. In these two configurations, the denominator of equation (16) must be calculated from the simulation output, but, with specified mole fractions everywhere, the denominator is known a priori from the imposed perturbation. Despite these differences, all configurations produce consistent estimates of $R=-0.270$ to -0.271 and $f=1.369$ to 1.372 (Table 1). Although the differences are very slight, the configuration with CH_4 emissions has the strongest feedback. That is because the CH_4 perturbation grows slightly larger in regions where CH_4 is most effective at suppressing OH, which is primarily the tropical marine atmosphere (see section 3.3), leading to further OH suppression and CH_4 accumulation. With prescribed concentrations, this cannot happen. While the boundary condition choice has a detectable effect on f, the differences are so slight (0.2%) that they are unlikely to matter for any application.

In the configuration with CH_4 emissions, equation (12) predicts that the simulation with 1.2 times greater emissions should eventually reach a steady state with $1.2^f=1.284$ times greater CH_4 mass. After 9 years of simulation, the model has not reached this state (Figure 1), but the time series fits an exponential approach to steady state with a value of $f=1.372 \pm 0.001$. This demonstrates the consistent estimates of feedback derived from multidecadal simulations (Figure 1) versus simulations of 2 years interpreted with equations (4) and (16) (Table 1). The multidecadal approach requires an order of magnitude more computational time, however, only works in models using CH_4 emissions, and appears to be unnecessary.

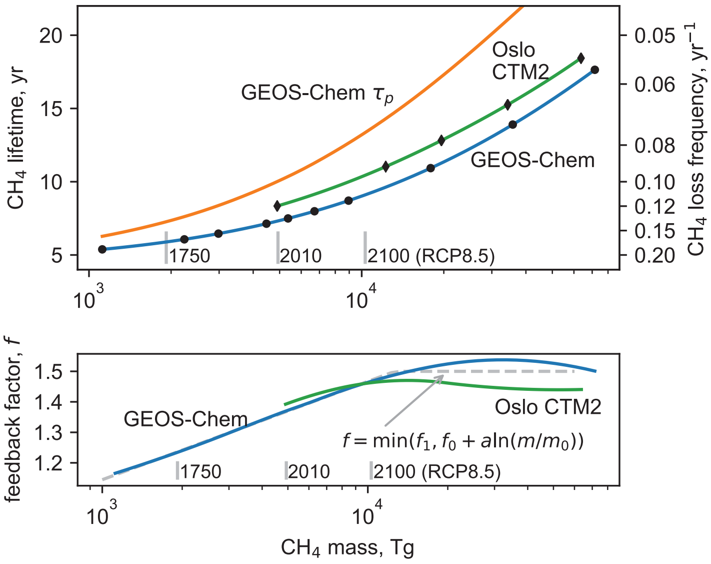

Figure 2. Simulated CH_4 lifetime, loss frequency, and perturbation time (top) and feedback factor (bottom) for a range of CH_4 burdens in the atmosphere. Simulated f values follow the inset equation and dashed line with $f_0=1.37$, $f_1=1.5$, $a=0.14$, and $m_0=5,000$ Tg. Meteorology and emissions of other compounds are held constant in all simulations. Gray ticks show the atmospheric CH_4 mass in 1750 and 2010, and projected mass in 2,100 in RCP8.5 (van Vuuren et al., 2011).

3.2. Stability of the Feedback Factor

The CH_4 feedback factor is sometimes treated as constant in time (e.g., section 1.3) but it is not (Isaksen et al., 2011; Prather et al., 1995). While changes in the CH_4 lifetime, τ, due to emissions and climate have been studied extensively in observations and models (e.g., Holmes et al., 2013; Montzka et al., 2011; Naik et al., 2013; Rigby et al., 2017; Turner et al., 2017; Voulgarakis et al., 2013), less attention has been given to temporal changes in f or τ_p, despite their importance to the climate impact of CH_4 (equation (6)).

Figure 2 shows the simulated CH_4 lifetime in a series of GEOS-Chem simulations with CH_4 mole fractions fixed at 0.25 to 16 times present-day. Each simulation runs for 2 years with 2006–2007 meteorology and the second year is analyzed. These simulations only modify CH_4 so they do not represent the full effects of historical or future changes in atmospheric composition. Isaksen et al. (2011) reported similar experiments in the Oslo CTM2, so those are also included. Simulations are fit with a cubic spline, which can be differentiated to obtain R and the feedback factor f.

The feedback factor in GEOS-Chem is $f = 1.37$ in the present-day simulation, but falls to 1.23 at 1750 levels of CH_4 and rises to a plateau of 1.45–1.55 at 2.5 times present-day CH_4. CTM2 predicts very similar trends in f over their overlapping range of CH_4 burden. The plateau occurs simply because, at high CH_4, k_{OH} becomes small and comparable to other losses ($k_{Cl}+k_{strat}+k_{soil}$). Beyond that point, equation (18) dictates that R and f stop increasing even though R_{OH} continues strengthening. The overall feedback becomes sensitive to feedbacks on other loss processes (R_{Cl}, R_{strat}, and R_{soil}). This behavior of f over the range $m=(1-60)\times 10^3$ Tg can reasonably be described as

$$f=\min\left(f_1, f_0+a\ \ln\left(m/m_0\right)\right), \tag{20}$$

where $f_0=1.37$, $f_1=1.5$, $a=0.14$, and $m_0=5,000$ Tg. Over the same range of mass, R_{OH} is described by $R_{OH}=0.49(m/m_0)^{-0.2}-0.81$, with 6% error or less. These functions enable numerical integration of equation (11) without the assumption of constant f implicit in equations (12) and (13).

Clearly, f is an increasing function of CH_4 burden from the preindustrial era through the twenty-first century for a range of scenarios, although the feedback factor has likely remained within about 10% of its present-day value. While f also depends on emissions, section 3.3 shows that the sensitivity to NO_x emissions is quite weak so the evolving CH_4 burden has likely been the main driver of historical changes in f. This historical rise in f in the single model here is larger than the range of f derived from model ensembles for the present (Fiore et al., 2009; Stevenson et al., 2013). Over the same range of CH_4 burden, the lifetime τ rises 55% from 5.9 to 9.2 year and the perturbation time τ_p rises nearly 90% from 7.3 to 13.7 year, because the CH_4 lifetime τ rises together with feedback factor f. Unlike f, the perturbation time does not reach a plateau at high CH_4 burden. Other things being equal, the CH_4 AGWP and environmental impacts scale with τ_p or with burden times τ_p, and therefore increase by 90% or more.

On short times scales, assuming constant feedback f is reasonable. The year-to-year variability in f, which can be diagnosed from the 9 year simulation in Figure 1, depends primarily on the changes in CH_4 burden. After removing the influence of rising CH_4 predicted by equation (20), the residual interannual variability in f is 0.002 (rms) or 0.2% of the mean. From a similar 13 year simulation in the UCI CTM (Holmes et al., 2013), the interannual variability of f is 0.3% in that model. This is the combined influence of variability in meteorology and emissions, meaning that both individually must have a small influence on the feedback, except insofar as they cause changes in the CH_4 burden. In comparison, meteorology and emissions drive much larger interannual variability in the CH_4 lifetime (1–2%, Holmes et al., 2013; Montzka et al., 2011; Murray et al., 2013).

3.3. Chemical Mechanism of the CH_4 Feedback and Its Regional Variability

Past literature has always described and quantified the CH_4 feedback as a global quantity. In reality, however, the OH response to CH_4 perturbations varies regionally and temporally. While a global value is sufficient for many applications, understanding this regional variability is probably required to develop observational tests of the simulated CH_4 feedback.

Figure 3 maps the feedback term R_{OH} geographically, seasonally, and vertically. R_{OH} is shown rather than R because this model only simulates the tropospheric OH loss. The figure shows just 1 month, June 2007, to avoid confounding effects of the seasonal cycle and because the processes are similar in all months. The feedback is strongest ($R_{OH} \approx -0.35$ to -0.4) over the tropical and subtropical oceans and generally weaker over land, although it remains strong over the Sahara and central Asia. The weakest feedback ($R_{OH} \approx -0.15$ to -0.25) occurs over the tropical continents, at the poles, and in the upper troposphere. For comparison, the CH_4 loss frequency k_{OH} is also large over the tropical oceans, but, whereas R_{OH} peaks over remote ocean basins, k_{OH} peaks in polluted coastal environments—where the mixture of O_3 pollution, water vapor, and sunlight provide a large primary source of OH via $O(^1D)$. CH_4 loss and feedback both peak in the summer hemisphere, but the seasonal cycle amplitude is much greater for k_{OH} than for R_{OH}. Globally, the feedback is slightly stronger in July than January, but the peak-to-peak change in global R_{OH} is only 0.02. At high latitudes and altitudes, k_{OH} is neglible because of the strong temperature dependence of reaction (1), but R_{OH} remains modest in these environments. The global value of $R_{OH} = -0.32$ (section 3.1, Table 1) is an average of the column values seen in Figure 3 weighted by the local k_{OH}. Thus, the global feedback is mainly determined by the feedback strength in the tropical lower troposphere, where k_{OH} is high.

The CH_4 feedback is usually explained as an increase in OH loss (reaction (1)) under constant OH sources (Prather, 1994, 1996, 2007) even though those sources could change. The model here can separately

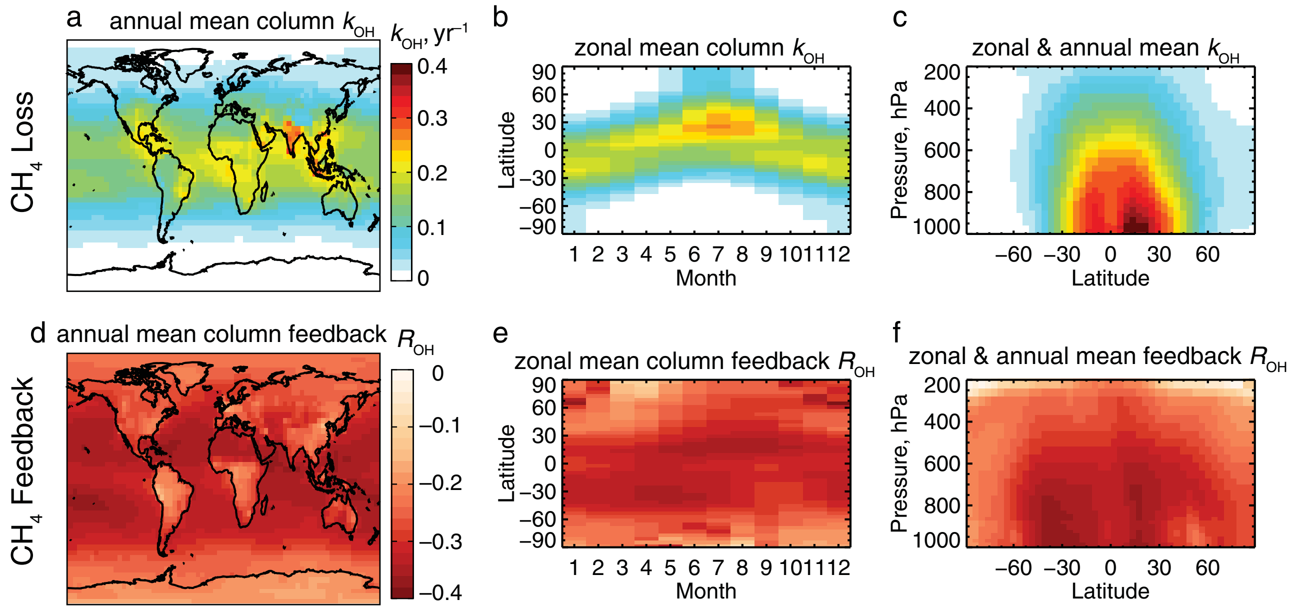

Figure 3. Spatial and seasonal distributions of CH_4 loss due to (a–c) tropospheric OH and the (d–f) CH_4 feedback. Plots a and d show annual averages for the tropospheric column. Plots b and e are hovmoller diagrams of the seasonal cycle. Plots c and f show zonal and annual means.

quantify the roles of OH losses versus sources in shaping the feedback strength. Globally, CH_4 directly consumes 15% of tropospheric OH (reaction (1)) and indirectly consumes about 40% of tropospheric OH after accounting for CO and other organic products of CH_4 oxidation that react with OH. In the remote marine lower troposphere, which has strong influence on the overall global feedback, CH_4 directly and indirectly consumes over 90% of OH in the model. If OH sources were constant, the effect of CH_4 perturbations on OH loss would generate a feedback of $-0.4 \geq R_{OH} \geq -0.9$. This is much larger than model's actual global value $R_{OH}=-0.32$, meaning that the feedback mechanism involves rising OH sources that offset about half of the additional OH loss.

To understand the spatial and seasonal patterns in Figure 3, it is helpful to consider the OH change at any location as a product of changes in HO_x family partitioning and the HO_x abundance ($HO_x = OH + HO_2$):

$$\frac{\Delta[\mathrm{OH}]}{[\mathrm{OH}]}=\frac{\Delta[\mathrm{HO_x}]}{[\mathrm{HO_x}]}+\frac{\Delta([\mathrm{OH}]/[\mathrm{HO_x}])}{[\mathrm{OH}]/[\mathrm{HO_x}]}. \qquad (21)$$

The CH_4 feedback is strong where this sum has a large negative magnitude. Figure 4 decomposes the CH_4 feedback in the lower troposphere into these two terms. This decomposition reveals that the $[OH]/[HO_x]$ ratio decreases 5–12% almost everywhere in response to the 20% increase in CH_4 abundance. The only exceptions are densely vegetated forests, mainly in the tropics and boreal zone. The change in HO_x ratio is offset in most places by a 3–10% increase in HO_x abundance. From this perspective, the CH_4 feedback is a balance between OH conversion to HO_2 versus overall increase in the HO_x abundance. Both components are similar magnitude, but the HO_x partitioning effect is stronger so overall CH_4 depletes OH. Nothing in the chemistry, however, requires that the OH change is negative; in the upper troposphere, CH_4 enhances OH for reasons explained below.

The $[OH]/[HO_x]$ ratio in the lower troposphere is primarily controlled by OH loss in reaction (1) and (Lelieveld et al., 2016)

$$\mathrm{OH+CO\xrightarrow{O_2}CO_2+HO_2} \qquad (22)$$

$$\mathrm{OH+RH\xrightarrow{O_2}RO_2+H_2O} \qquad (23)$$

balanced by OH production from

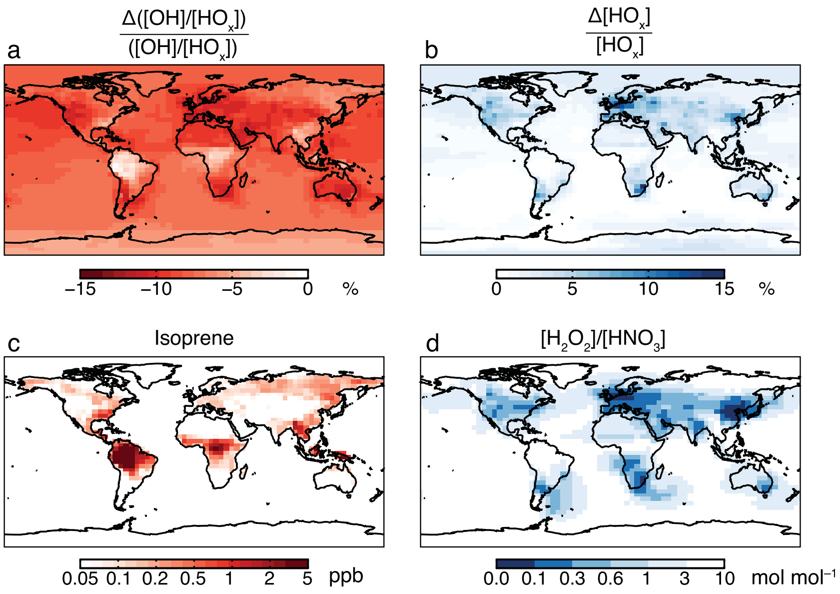

Figure 4. Chemical response in the lower troposphere to a 20% increase in atmospheric CH_4: (a) change in the $[OH]/[HO_x]$ ratio, (b) change in the $[HO_x]$ abundance. Chemical factors that influence those changes: (c) isoprene abundance, (d) $[H_2O_2]/[HNO_3]$ ratio. All quantities are averages over the lowest 13 model layers where pressure $\gtrsim$800 hPa in June 2007.

$$O_3 + hv \rightarrow O(^1D) + O_2 \tag{24}$$

$$O(^1D) + H_2O \rightarrow 2OH \tag{25}$$

$$HO_2 + NO \rightarrow OH + NO_2 \tag{26}$$

$$HO_2 + O_3 \rightarrow OH + 2O_2. \tag{27}$$

From these reactions, and recognizing that $[HO_x] \approx [HO_2]$, the HO_x family partitioning is

$$\frac{[OH]}{[HO_x]} \approx \frac{k_{26}[NO] + k_{27}[O_3] + k_{25}\left[O(^1D)\right][H_2O]/[HO_x]}{k_1[CH_4] + k_{22}[CO] + k_{23}[RH]}. \tag{28}$$

In high-NO_x environments, reaction (26) typically dominates OH production, so equation (28) can be simplified by neglecting reactions (25) and (27). The analysis here, however, focuses on how the competing reactions in the denominator impact the sensitivities in equation (21) and Figure 4.

Equation (28) predicts that the HO_x partitioning should be insensitive to CH_4 in environments with high hydrocarbon concentrations, meaning that $k_{23}[RH]$ controls the denominator. Indeed, Figure 4 shows that the $[OH]/[HO_x]$ ratio changes very little where isoprene and other biogenic hydrocarbon concentrations are high. Over tropical and boreal forests, biogenic emissions in the model consume 40–70% of the OH in the lower troposphere and CH_4 consumes less than 10%, consistent with the low sensitivity of $[OH]/[HO_x]$ to CH_4.

Figure 4 also shows that the CH_4 perturbation over industrial regions generates large HO_x increases that offset 80% of the reduction in $[OH]/[HO_x]$ ratio. Over the ocean, the offset is less than 30%. These industrial areas have major anthropogenic NO_x emissions and the ratio $[H_2O_2]/[HNO_3] \lesssim 0.3$, an indicator for NO_x-saturated O_3 production (Jacob et al., 1995; Sillman, 1995), is a good predictor of where the offset peaks. The model can explain the HO_x increase by diagnosing the reactions that contribute to HO_y production ($HO_y = HO_x$ + reservoirs $= HO_x + HNO_2 + HNO_4 + HOBr + 2H_2O_2$ + organic peroxy radicals + 2 × organic peroxides + peroxyacyl nitrates). The CH_4-driven rise in HO_x abundance comes from three HO_y sources (supporting information Figure S1): (1) direct production from CH_4 oxidation products ($CH_2O + hv \xrightarrow{O_2} CO + 2HO_2$), (2) indirect production from CH_4-derived O_3 through reactions (24) and (25), and (3) autocatalytic amplification of (1) and (2) through VOC oxidation (Wennberg et al., 1998).

Indirect HO_y production via CH_4-derived O_3 supplies nearly all of the HO_x increase seen in Figure 4 over the tropical oceans, but just 10% over the industrial continents (supporting information Figure S1). The direct source generates 0.2–0.6 mole of HO_y for each mole of CH_4 oxidized in the lower troposphere. This explains 40% of the HO_x increase in the Arctic but less than 20% everywhere else. Adding the direct and indirect sources together explains all of the HO_x increase over the oceans, but only about 30% over industrial continents. Autocatalytic amplification explains the rest of the HO_x increase. The amplification factor can be diagnosed in the model from total HO_y production in the control simulation divided by noncatalytic HO_y production: reaction (25), ozonolysis of VOC, and photolysis of emitted aldehydes and ketones (Jaeglé et al., 2001; Wennberg et al., 1998). This analysis shows that HO_y sources are amplified by a factor of 4–5 in NO_x-rich continental regions but have almost zero amplification (factor 1–1.5) over oceans and land regions where $[H_2O_2]/[HNO_3] \gtrsim 0.6$ (supporting information Figure S1). Combining the amplified direct and indirect HO_y sources quantitatively explains the global pattern and magnitude of HO_x changes produced by the CH_4 perturbation (Figure 4 and supporting information Figure S1). Thus, the large HO_x increase and weak CH_4 feedback over the industrial continents is mostly (70–80%) explained by autocatalytic HO_y production that is enabled by NO_x-saturated conditions. The strongest feedback, meaning most negative R_{OH}, coincides with regions where $O(^1D) + H_2O$ (reaction (25)) dominates OH supply and the numerator of equation (28). These features coincide because under low-NO_x conditions, such as the tropical oceans and some deserts, HO_2 recycling to OH is very limited (e.g., Lelieveld et al., 2016), which leaves $O(^1D) + H_2O$ as the main OH source. At the same time, low-NO_x conditions also make autocatalytic HO_x production ineffective, so there is little HO_x increase when CH_4 concentrations rise; as a result, R_{OH} is strongly negative.

The feedback mechanism operates differently in polar regions and in the upper troposphere. Near the poles, the feedback is weak ($R_{OH} \approx -0.2$), despite negligible biogenic emissions and low NO_x levels. At the poles, the CH_4 perturbation depresses $[OH]/[HO_x]$ just as it does elsewhere, but the HO_x offset is much larger than might be expected from the large $[H_2O_2]/[HNO_3]$ ratio. The reason is that CH_2O photolysis is a major HO_y source near the poles, unlike the lower latitudes (Mao et al., 2010). As a result, CH_4 perturbations produce a large relative increase in HO_x via CH_2O, without requiring NO_x for autocatalytic amplification or major changes in O_3. In the upper troposphere ($p < 200$ hPa), R_{OH} is slightly positive ($0 \leq R_{OH} \leq 0.1$), meaning that rising CH_4 increases OH, unlike the rest of the troposphere. In this region, CH_4 oxidation is an important HO_x source (Wennberg et al., 1998) and the $[OH]/[HO_x]$ ratio has very little sensitivity to CH_4 because reaction (1) has strong temperature dependence. While interesting, the upper troposphere and polar feedback has little impact on the overall global feedback because k_{OH} is very small in these regions.

3.4. Meteorological and Emission Controls on the Global CH_4 Feedback Strength

Table 2 summarizes the effects of meteorology and selected emissions on the global CH_4 feedback. For comparison, past studies have found that temperature, radiation, humidity, and NO_x all strongly increase CH_4 loss by tropospheric OH (k_{OH}), while emissions of CO and nonmethane volatile organic compounds (NMVOC) weakly decrease it (Holmes et al., 2013). The same meteorological variables have much weaker influence on the feedback strength. In explicit sensitivity tests here, increasing water vapor mole fractions or photolysis rates by 20% increase the feedback just 1%. A 1 K increase in temperature has no effect on the feedback. These sensitivity tests involve changes that exceed interannual variability and are at the upper end of expected decadal changes under greenhouse gas forcing. Actual interannual variability in the feedback strength driven by meteorology should therefore be under 1%, in agreement with the small variability found in the multiyear simulation (section 3.2). The weak sensitivity of the feedback to insolation, water vapor, and temperature is also consistent with the weak seasonal cycle in f and weak vertical and meridional gradients seen in Figure 3.

Table 2

Effect of Meteorological and Chemical Variables on the CH_4 Loss Frequency (k_{OH}) and CH_4 Feedback (f)[a]

Variable	k_{OH}	f
Insolation	++	+
Temperature	++	=
Humidity	++	+
NO_x emission	++	=[b]
CO, NMVOC emission	−	−−

[a] Symbols indicate how the process responds to increases in the variable: strongly positive (++), modestly positive (+), weak or variable (=), modestly negative (−), and strongly negative (−−). Effects on k_{OH} are from Holmes et al. (2013). Effects on f are from this work. [b] NO_x emissions locally weaken the feedback near the source but globally strengthen it very slightly (section 3.4).

Hydrocarbon and CO emissions clearly weaken the CH_4 feedback via equation (28). The sensitivity test with doubled CO emissions confirms this, dropping the feedback from $f = 1.37$ to $f = 1.31$. NO_x emissions are more complex, however. While Figure 4 shows that the CH_4 feedback is weak in regions with large NO_x emissions, the explicit sensitivity test reveals that raising NO_x emissions above present-day levels actually strengthens the feedback. Doubling NO_x emissions drives the feedback up 0.02 to $f = 1.39$. For such a large change in NO_x emissions, this is a weak effect. In contrast, this same NO_x emission change boosts k_{OH} by 22%. Spatially, doubling NO_x weakens the CH_4 feedback over source regions, but strengthens it everywhere else. The reason is NO_x emissions raise mean levels of tropospheric O_3 and OH. As a result, in an emission-driven simulation, background CO and CH_4 concentrations fall by similar fractions, but slightly more for CO than CH_4 due to their spatial distributions relative to OH, so equation (28) becomes slightly more sensitive to CH_4 over most of the globe. Voulgarakis et al. (2013) reported that climate models predict strengthening CH_4 feedback over the twenty-first century in the RCP8.5 climate scenario. They hypothesized that declining anthropogenic NO_x emissions could explain the effect, but this work shows that NO_x has the opposite or perhaps zero effect. Instead, the strengthening feedback in RCP8.5 is more likely due to the projected doubling of CH_4 abundance in that scenario through the processes explained in section 3.2.

4. Conclusions

The CH_4 feedback on atmospheric chemistry, in which tropospheric OH concentrations fall as CH_4 abundance rises, is a major climate process, responsible for about 30% of the CH_4 radiative forcing or 0.3 W m^{-2} in 2011. This article reviews the feedback theory, applications, and modeling methods, then explores new aspects of the CH_4 feedback. The mechanism for falling OH concentrations is often described simply as a rise in OH loss due to rising CH_4 and the CO it produces. This is only partly correct, however, since rising CH_4 also boosts HO_x sources. Global model simulations here show that the rise in HO_x abundance offsets about half of the reduction in OH/HO_x ratio caused by CH_4 perturbations.

The CH_4 feedback strength varies geographically and seasonally. It is strongest over the oceans and in the summer hemisphere and low over tropical forests and industrial regions. While these patterns in the feedback have not been previously described, they can be explained in terms of well-known chemistry of HO_x partitioning and production. The CH_4 feedback is weak where NMVOC emissions are large, because the $[OH]/[HO_x]$ ratio becomes insensitive to CH_4, and also weak where NO_x emissions are large, because additional HO_y production balances the change in HO_x partitioning. It may be possible to construct indirect or emergent observational tests of the CH_4 feedback strength based on geographic extent of these chemical regimes, and OH reactivity, $[OH]/[HO_x]$, and HO_x budgets in each. Testing these features has been a longstanding goal of atmospheric chemistry measurements and modeling, but tightening constraints on the CH_4 feedback and lifetime likely requires greater focus on evaluating models in the coastal zones at low latitudes, which have the greatest influence on the global feedback.

Global atmospheric chemistry models use either surface flux or specified concentration boundary conditions for CH_4. Although CH_4 perturbations behave slightly differently in these configurations, the subtle differences are unlikely to matter for any application. Consequently, the differences seen in ensembles of models with a mix of these boundary conditions must arise from their different meteorology and chemistry, not an artifact of their boundary conditions (Fiore et al., 2009; Naik et al., 2013; Stevenson et al., 2013; Voulgarakis et al., 2013). These ensemble studies have focused almost entirely on the CH_4 feedback through tropospheric oxidant chemistry. CH_4 feedbacks through the chlorine, soil, and stratosphere sinks, or natural emissions could raise or lower the feedback factor f and the perturbation time. With the exception of some carbon cycle effects (Myhre et al., 2013), these additional feedbacks have not been evaluated, but they are potentially relevant for mitigation planning that involves tradeoffs between greenhouse gases using GWP or other impact metrics.

Explicit sensitivity tests show that the global CH_4 feedback strength depends only weakly on temperature, water vapor, insolation, and NO_x emissions, but robustly strengthens as CH_4 rises or NMVOCs fall. As a result, the feedback is very stable from year to year. This weak sensitivity may also explain why model ensembles seem to predict a narrow range of f despite their larger range of k_{OH} (3% versus 10%, respectively, Stevenson et al., 2013; Voulgarakis et al., 2013). Over decades and longer, changes in CH_4 abundance alter the feedback strength. The feedback strength increases from $f = 1.23$ at preindustrial CH_4 levels to $f = 1.45$ at twice present levels. This is $\pm 10\%$ of present-day feedback over a fivefold change in atmospheric CH_4 burden. The feedback is only weakly sensitive to the historical changes in O_3 precursor emissions and climate that have accompanied the rise in atmospheric CH_4. Given these modest changes it may be acceptable for some applications in the recent past and near future to treat the feedback factor f as a constant, but this introduces a systematic bias in the results. The environmental and climate warming impacts of CH_4 are generally proportional to the perturbation time $\tau_p = f\tau$ and both f and τ increase with CH_4 concentration. Considering the effects of CH_4 burden alone, τ_p may have risen 40% over the industrial era and up to 90% by the end of the twenty-first century. As a result, accurate climate and environmental assessments require accounting for the evolution of CH_4 GWP and other environmental impacts.

Acknowledgments
C.D.H. thanks an anonymous reviewer and Michael Prather for comments on an early draft. This work was supported by the NASA New-Investigator Program through grant NNX16AI57G. Model output used to calculate the CH_4 feedback is provided in the supplement. GEOS-Chem source code used here is archived at Zenodo, https://doi.org/10.5281/zenodo.1208708.

References

Berntsen, T., Isaksen, I. S. A., & Fuglestvedt, J. S. (1992). Chemical-dynamical modelling of the atmosphere with emphasis on the methane oxidation. *Berichte der Bunsengesellschaft für physikalische Chemie*, *96*(3), 241–251. http://doi.org/10.1002/bbpc.19920960303

Derwent, R., Collins, W., Johnson, C., & Stevenson, D. (2001). Transient behaviour of tropospheric ozone precursors in a global 3-D CTM and their indirect greenhouse effects. *Climatic Change*, *49*(4), 463–487.

Dlugokencky, E. J., Lang, P. M., Crotwell, A. M., Mund, J. W., Crotwell, M. J., et al. (2017). *Atmospheric methane dry air mole fractions from the NOAA ESRL carbon cycle cooperative global air sampling network, 1983–2016*. Boulder, CO: National Oceanic and Atmospheric Administration Earth System Research Laboratory (NOAA ESRL). Retrieved from ftp://aftp.cmdl.noaa.gov/data/trace_gases/ch4/flask/surface/, accessed 28 July 2017

Fiore, A. M., Dentener, F. J., Wild, O., Cuvelier, C., Schultz, M. G., Hess, P., et al. (2009). Multimodel estimates of intercontinental source-receptor relationships for ozone pollution. *Journal of Geophysical Research: Atmospheres*, *114*, D04301. http://doi.org/10.1029/2008JD010816

Fuglestvedt, J. S., Berntsen, T. K., Isaksen, I., Mao, H. T., Liang, X. Z., & Wang, W.-C. (1999). Climatic forcing of nitrogen oxides through changes in tropospheric ozone and methane; global 3D model studies. *Atmospheric Environment*, *33*(6), 961–977.

Fuglestvedt, J. S., Isaksen, I., & Wang, W.-C. (1996). Estimates of indirect global warming potentials for CH_4, CO and NO_x. *Climatic Change*, *34*(3–4), 405–437.

Gelaro, R., McCarty, W., Suarez, M. J., Todling, R., Molod, A., Takacs, L., et al. (2017). The modern-era retrospective analysis for research and applications, Version 2 (MERRA-2). *Journal of Climate*, *30*(14), 5419–5454. http://doi.org/10.1175/JCLI-D-16-0758.1

Holmes, C. D., Prather, M. J., Søvde, O. A., & Myhre, G. (2013). Future methane, hydroxyl, and their uncertainties: Key climate and emission parameters for future predictions. *Atmospheric Chemistry and Physics*, *13*(1), 285–302. http://doi.org/10.5194/acp-13-285-2013

Isaksen, I. S. A., Gauss, M., Myhre, G., Anthony, K. M. W., & Ruppel, C. (2011). Strong atmospheric chemistry feedback to climate warming from Arctic methane emissions. *Global Biogeochemical Cycles*, *25*, GB2002. http://doi.org/10.1029/2010GB003845

Jacob, D. J., Horowitz, L. W., Munger, J. W., Heikes, B. G., Dickerson, R. R., Artz, R. S., et al. (1995). Seasonal transition from NO_{x-} to hydrocarbon-limited conditions for ozone production over the eastern United States in September. *Journal of Geophysical Research*, *100*(D5), 9315–9324. http://doi.org/10.1029/94JD03125

Jaeglé, L., Jacob, D. J., Brune, W. H., & Wennberg, P. O. (2001). Chemistry of HO_x radicals in the upper troposphere. *Atmospheric Environment*, *35*, 469–489. http://doi.org/10.1016/S1352-2310(00)00376-9

Lelieveld, J., Gromov, S., Pozzer, A., & Taraborrelli, D. (2016). Global tropospheric hydroxyl distribution, budget and reactivity. *Atmospheric Chemistry and Physics*, *16*(19), 12477–12493. http://doi.org/10.5194/acp-16-12477-2016

Mao, J., Jacob, D. J., Evans, M. J., Olson, J. R., Ren, X., Brune, W. H., et al. (2010). Chemistry of hydrogen oxide radicals (HO_x) in the Arctic troposphere in spring. *Atmospheric Chemistry and Physics*, *10*(13), 5823–5838. http://doi.org/10.5194/acp-10-5823-2010

Montzka, S. A., Krol, M., Dlugokencky, E., Hall, B., Joeckel, P., & Lelieveld, J. (2011). Small interannual variability of global atmospheric hydroxyl. *Science*, *331*, 67–69. http://doi.org/10.1126/science.1197640

Murray, L. T., Logan, J. A., & Jacob, D. J. (2013). Interannual variability in tropical tropospheric ozone and OH: The role of lightning. *Journal of Geophysical Research: Atmospheres*, *118*, 11468–11480. http://doi.org/10.1002/jgrd.50857

Myhre, G., Shindell, D., Breon, F. M., Collins, W., Fuglestvedt, J., Huang, J., et al. (2013). Anthropogenic and natural radiative forcing. In Stocker, T. F., Qin, D., Plattner, G. K., Tignor, M., Allen, S. K., Boschung, J., et al. (Eds.), *Climate change 2013: The physical science basis. contribution of working group I to the fifth assessment report of the intergovernmental panel on climate change* (pp. 659–740). Cambridge, UK: Cambridge University Press.

Naik, V., Voulgarakis, A., Fiore, A. M., Horowitz, L. W., Lamarque, J. F., Lin, M., et al. (2013). Preindustrial to present-day changes in tropospheric hydroxyl radical and methane lifetime from the Atmospheric Chemistry and Climate Model Intercomparison Project (ACCMIP). *Atmospheric Chemistry and Physics*, *13*(10), 5277–5298. http://doi.org/10.5194/acp-13-5277-2013

Parrella, J. P., Jacob, D. J., Liang, Q., Zhang, Y., Mickley, L. J., Miller, B., et al. (2012). Tropospheric bromine chemistry: Implications for present and pre-industrial ozone and mercury. *Atmospheric Chemistry and Physics*, *12*(15), 6723–6740. http://doi.org/10.5194/acp-12-6723-2012

Prather, M. (1994). Lifetimes and eigenstates in atmospheric chemistry. *Geophysical Research Letters*, *21*(9), 801–804. http://doi.org/10.1029/94GL00840

Prather, M. (2002). Lifetimes of atmospheric species: Integrating environmental impacts. *Geophysical Research Letters*, *29*(22), 2063. http://doi.org/10.1029/2002GL016299

Prather, M. J. (2007). Lifetimes and time scales in atmospheric chemistry. *Philosophical Transactions of the Royal Society A*, *365*(1856), 1705–1726. http://doi.org/10.1098/rsta.2007.2040

Prather, M., Derwent, R., Ehhalt, D., Eraser, P., Sanhueza, E., Zhou, X., et al. (1995). Other trace gases and atmospheric chemistry. In Houghton, J., Meira Filho, L. G., Bruce, J., Lee, H., Callander, B. A., & Haites, E. (Eds.), *Climate change 1994*. (pp. 73–126). Cambridge, UK: Cambridge University Press.

Prather, M., Ehhalt, D., Dentener, F., Derwent, R., Dlugokencky, E., Holland, E., et al. (2001). Atmospheric chemistry and greenhouse gases. In Houghton, J., Ding, Y., Griggs, D., Noguer, M., van der Linden, P., Dai, X., et al. (Eds.), *Climate change 2001: The scientific basis. Third assessment report of the intergovernmental panel on climate change*. Cambridge, UK: Cambridge University Press.

Prather, M., Holmes, C., & Hsu, J. (2012). Reactive greenhouse gas scenarios: Systematic exploration of uncertainties and the role of atmospheric chemistry. *Geophysical Research Letters*, *39*, L09803. http://doi.org/10.1029/2012GL051440

Rigby, M., Montzka, S. A., Prinn, R. G., White, J. W. C., Young, D., O'Doherty, S., et al. (2017). Role of atmospheric oxidation in recent methane growth. *Proceedings of the National Academy of Sciences of the United States of America*, *114*(21) 5373–5377. http://doi.org/10.1073/pnas.1616426114

Sherwen, T., Schmidt, J. A., Evans, M. J., Carpenter, L. J., Großmann, K., Eastham, S. D., et al. (2016). Global impacts of tropospheric halogens (Cl, Br, I) on oxidants and composition in GEOS-Chem. *Atmospheric Chemistry and Physics*, *16*(18), 12239–12271. http://doi.org/10.5194/acp-16-12239-2016

Sillman, S. (1995). The use of NO_y, H_2O_2, and HNO_3 as indicators for ozone-NO_x-hydrocarbon sensitivity in urban locations. *Journal of Geophysical Research*, *100*(D7), 14175–14188. http://doi.org/10.1029/94JD02953

Spivakovsky, C., Logan, J., Montzka, S., Balkanski, Y., Foreman-Fowler, M., Jones, D., et al. (2000). Three-dimensional climatological distribution of tropospheric OH: Update and evaluation. *Journal of Geophysical Research*, *105*(D7), 8931–8980. http://doi.org/10.1029/1999JD901006

Stevenson, D. S., Young, P. J., Naik, V., Lamarque, J. F., Shindell, D. T., Voulgarakis, A., et al. (2013). Tropospheric ozone changes, radiative forcing and attribution to emissions in the Atmospheric Chemistry and Climate Model Intercomparison Project (ACCMIP). *Atmospheric Chemistry and Physics*, *13*(6), 3063–3085. http://doi.org/10.5194/acp-13-3063-2013

Turner, A. J., Frankenberg, C., Wennberg, P. O., & Jacob, D. J. (2017). Ambiguity in the causes for decadal trends in atmospheric methane and hydroxyl. *Proceedings of the National Academy of Sciences of the United States of America*, *44*, 201616020. http://doi.org/10.1142/3171

van Vuuren, D. P., Edmonds, J., Kainuma, M., Riahi, K., Thomson, A., Hibbard, K., et al. (2011). The representative concentration pathways: An overview. *Climatic Change*, *109*, 5–31. http://doi.org/10.1007/s10584-011-0148-z

Voulgarakis, A., Naik, V., Lamarque, J. F., Shindell, D. T., Young, P. J., Prather, M. J., et al. (2013). Analysis of present day and future OH and methane lifetime in the ACCMIP simulations. *Atmospheric Chemistry and Physics*, *13*(5), 2563–2587. http://doi.org/10.5194/acp-13-2563-2013

Wecht, K. J., Jacob, D. J., Frankenberg, C., Jiang, Z., & Blake, D. R. (2014). Mapping of North American methane emissions with high spatial resolution by inversion of SCIAMACHY satellite data. *Journal of Geophysical Research: Atmospheres*, *119*, 7741–7756. http://doi.org/10.1002/gbc.20052

Wennberg, P. O., Hanisco, T. F., Jaegle, L., Jacob, D. J., Hintsa, E. J., Lanzendorf, E. J., et al. (1998). Hydrogen radicals, nitrogen radicals, and the production of O_3 in the upper troposphere. *Science*, *279*, 49–53. http://doi.org/10.1126/science.279.5347.49

West, J. J., Fiore, A. M., Naik, V., Horowitz, L. W., Schwarzkopf, M. D., & Mauzerall, D. L. (2007). Ozone air quality and radiative forcing consequences of changes in ozone precursor emissions. *Geophysical Research Letters*, *34*, L06806. http://doi.org/10.1029/2006GL029173

Wild, O., & Prather, M. (2000). Excitation of the primary tropospheric chemical mode in a global three-dimensional model. *Journal of Geophysical Research*, *105*(D20), 24647–24660. https://doi.org/10.1029/2000JD900399